Discovery and Characterization of Novel Subtype-Selective Allosteric Agonists for the Investigation of M_1 Receptor Function in the Central Nervous System

Evan P. Lebois,[†] Thomas M. Bridges,[†] L. Michelle Lewis,[†,§] Eric S. Dawson,[‡,§,⊥,∥] Alexander S. Kane,[†,⊥] Zixiu Xiang,[†,⊥] Satyawan B. Jadhav,[†,⊥] Huiyong Yin,[§] J. Phillip Kennedy,[‡] Jens Meiler,[‡,§,⊥,∥] Colleen M. Niswender,[†,⊥] Carrie K. Jones,[†,⊥] P. Jeffrey Conn,[†,§,⊥] C. David Weaver,[†,§,⊥] and Craig W. Lindsley*[,†,‡,§,⊥]

[†]Department of Pharmacology and [‡]Department of Chemistry and [§]Vanderbilt Specialized Chemistry Center for Accelerated Probe Development (MLPCN) and [⊥]Vanderbilt Program in Drug Discovery and [∥]Vanderbilt Center for Structural Biology, Vanderbilt University Medical Center, Nashville, Tennessee 37232-6600

Abstract

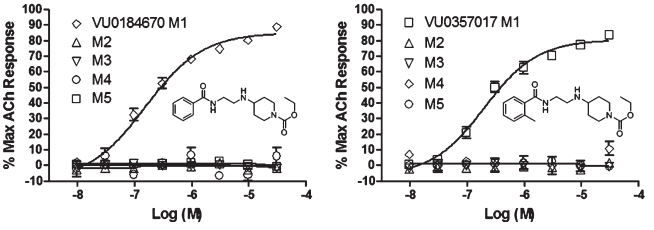

Cholinergic transmission in the forebrain is mediated primarily by five subtypes of muscarinic acetylcholine receptors (mAChRs), termed M_1-M_5. Of the mAChR subtypes, M_1 is among the most heavily expressed in regions that are critical for learning and memory and has been viewed as the most critical mAChR subtype for memory and attention mechanisms. Unfortunately, it has been difficult to develop selective activators of M_1 and other individual mAChR subtypes, which has prevented detailed studies of the functional roles of selective activation of M_1. Using a functional high-throughput screening and subsequent diversity-oriented synthesis approach, we have discovered a novel series of highly selective M_1 allosteric agonists. These compounds activate M_1 with EC_{50} values in the 150−500 nM range and have unprecedented, clean ancillary pharmacology (no substantial activity at 10 μM across a large panel of targets). Targeted mutagenesis revealed a potentially novel allosteric binding site in the third extracellular loop of the M_1 receptor for these allosteric agonists. Optimized compounds, such as VU0357017, provide excellent brain exposure after systemic dosing and have robust *in vivo* efficacy in reversing scopolamine-induced deficits in a rodent model of contextual fear conditioning. This series of selective M_1 allosteric agonists provides critical research tools to allow dissection of M_1-mediated effects in the CNS and potential leads for novel treatments for Alzheimer's disease and schizophrenia.

Keywords: mAChR, muscarinic, allosteric, agonist, cognition

The muscarinic acetylcholine receptors are members of the class A G-protein-coupled receptors (GPCRs) that mediate a broad range of actions of the neurotransmitter acetylcholine (ACh) in the central nervous system and other tissues. To date, five distinct subtypes of mAChRs (M_1-M_5) have been cloned and sequenced (*1*−*3*). M_1, M_3, and M_5 activate phospholipase C through G_q to stimulate calcium release, whereas M_2 and M_4 couple to inhibition of adenylyl cyclase and other effector systems through activation of $G_{i/o}$ (Figure 1A). Cholinergic neurotransmission mediated by mAChRs plays a critical role in a wide variety of CNS and peripheral functions including memory and attention mechanisms, motor control, nociception, regulation of sleep−wake cycles, cardiovascular function, renal and gastrointestinal function, and many others (*1*, *3*). As a result, agents that can selectively modulate the activity of mAChRs have the potential for therapeutic use in multiple pathological states (*4*−*12*). Based on brain expression and cellular localization, data from mAChR knockout mice and clinical trials with muscarinic agonists, the M_1 mAChR subtype is an attractive molecular target for the treatment of Alzheimer's disease (AD) and schizophrenia (*4*−*12*).

Previous attempts to develop compounds that are highly selective for M_1 or other specific mAChR subtypes have failed because of the high conservation of the orthosteric ACh binding site and difficulty in developing truly specific compounds (*13*). The lack of highly selective compounds has made it impossible to definitively determine the behavioral effects and potential clinical utility of selectively activating individual mAChR subtypes. In numerous phase II and III clinical trials, pan-mAChR agonists were shown to improve cognitive performance in AD patients, but the GI-and cardiovascular side effects, resulting from activation of peripheral

Received Date: August 12, 2009
Accepted Date: September 10, 2009
Published on Web Date: September 25, 2009

DOI: 10.1021/cn900003h | *ACS Chem. Neurosci.* (2010), *1*, 104–121

mAChRs, were deemed intolerable and the trials were discontinued (*13*, *14*). Importantly, evidence suggests that pan-mAChR agonists may also reduce Aβ42 levels in the cerebral spinal fluid of AD patients, suggesting that mAChR activation has the potential to be disease-modifying as well as providing palliative cognitive therapy (*9*, *13*, *15*−*22*). More recent studies in 3xTg-AD mice further support a disease-modifying role for mAChR activation (*23*). Interestingly, in addition to improving cognitive performance, the M_1/M_4-preferring xanomeline also had robust therapeutic effects on the psychotic symptoms and behavioral disturbances associated with AD, and recently published clinical data indicates that xanomeline has efficacy in treatment of positive and negative symptoms in schizophrenic patients (*11*, *22*). These findings provide strong support for the hypothesis that highly selective M_1 agonists may provide an exciting new approach for treatment of AD and schizophrenia. Recently, a detailed pharmacological comparison of known M_1 orthosteric agonists was described, and each of these compounds suffered from poor mAChR subtype selectivity, and all had significant ancillary pharmacology at biogenic amine receptors (dopamine, serotonin, histamine, etc.) (*13*). Unfortunately, this lack of selectivity for M_1 versus M_2−M_5 and multiple biogenic amine receptors precludes their use as tools to study M_1 function.

An alternative approach to targeting the highly conserved orthosteric ACh site is to develop compounds that act at allosteric sites on mAChRs that are removed from the orthosteric site and may be less highly conserved. This approach is proving highly successful for multiple GPCRs (*17*, *18*, *24*, *25*). For mAChRs, positive allosteric modulators, molecules that bind at an allosteric site, do not activate the receptor directly, but potentiate activation of the receptor by the orthosteric agonist ACh, have been reported for M_1, M_4, and M_5 (*17*, *18*, *26*−*28*). Alternatively, allosteric agonists, molecules that bind at an allosteric site and directly activate the receptor in the absence of ACh, have also been described (Figure 1B) for M_1 and include NDMC (**1**), AC-42 (**2**), 77-LH-28-1 (**3**), and TBPB (**4**) (*21*, *29*−*31*). Discovery of these novel M_1 allosteric agonists provides a major advance and suggests that it may be possible to discover highly selective and systemically active M_1 agonists by targeting allosteric sites; moreover, all of these allosteric ligands are believed to bind within the transmembrane (TM) domain of the GPCR (*31*, *32*). However, none of the novel M_1 allosteric agonists discovered to date are entirely selective for M_1, and each has limitations that diminish their use for probing the activity of this receptor in native preparations (*13*).

We now report discovery of VU0184670 and VU0357017 and related compounds as highly selective

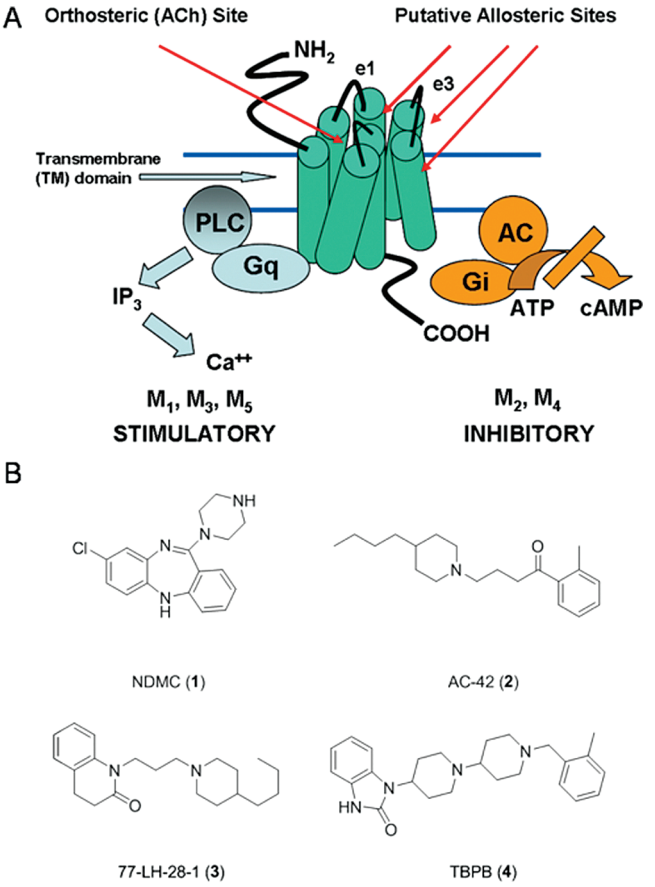

Figure 1. mAChR structure and known M_1 allosteric agonists: (A) schematic illustration of structure and effector systems of the mAChR subtypes M_1−M_5; (B) structures of known M_1 allosteric agonists NDMC (**1**), AC-42 (**2**), 77-LH-28-1 (**3**), and TBPB (**4**).

and systemically active M_1 allosteric agonists (see Figure 4A). These compounds have no detectable agonist activity at other mAChR subtypes and have favorable ancillary pharmacological profiles when evaluated in a large panel of GPCRs and other potential CNS targets (<50% inhibition at 10 μM). In addition to improvements in selectivity and ancillary pharmacology, these allosteric agonists show complete aqueous solubility (>25 mg/mL in H_2O) and favorable pharmacokinetic properties when dosed intraperitoneally (ip) in rats. Mutagenesis studies revealed that mutation of specific residues in the third extracellular loop of the M_1 receptor drastically decreased the functional potency of these ligands, implicating this novel region as critical for ligand−receptor interactions underlying activation. Finally, VU0184670 and VU0357017 are highly suitable for use in both CNS preparations and *in vivo* investigations, because they induced robust potentiation of NMDA receptor currents in hippocampal neurons and displayed efficacy in reversing deficits in cognitive function in a rodent behavioral model of hippocampal-dependent memory.

DOI: 10.1021/cn900003h | *ACS Chem. Neurosci.* (2010), *1*, 104–121

Results and Discussion

A major problem that has hampered the basic science efforts driving muscarinic research across all receptor subtypes is a lack of truly selective tool compounds to clearly elucidate the physiological role of given subtypes (*4*, *6*, *10*). This need becomes immediately apparent in the context of the mammalian CNS, where M_1 and M_4 expression predominate and there is urgent need to clearly define the relative contribution of each to various pathological processes such as AD and schizophrenia. Knockout studies performed in mice and other investigations generally have concluded that the M_1 receptor is the primary mediator of cognitive efficacy, while the M_4 subtype seems to underlie antipsychotic efficacy, with both of these receptors impinging upon processes intimately connected to learning, memory, synaptic plasticity, and higher cognitive function (*22*, *33*−*36*). Thus, over the past several decades, numerous drug discovery programs have ardently tried to develop selective M_1 activators, largely to no avail, by targeting the orthosteric site (*13*). Acetylcholinesterase inhibitors remain the only currently FDA-approved compounds for treating AD; however, these compounds merely present a means of palliative therapy, and there is no data at present to support a disease-modifying role (*37*, *38*). Notably, the most promising recent phase III clinical trial with the M_1/M_4-preferring agonist xanomeline demonstrated clinical proof of concept that targeting M_1/M_4 receptors resulted in cognitive improvement in AD patients, as well as efficacy in schizophrenia trials (*11*, *14*, *22*, *24*).

The Vanderbilt Screening Center for GPCRs, Ion Channels and Transporters and the companion Vanderbilt Specialized Chemistry Center were established as members of the Molecular Libraries Production Center Network (MLPCN) initiated and supported by the NIH Molecular Libraries Roadmap (*39*, *40*). The MLPCN is a nationwide consortium of facilities that provide high-throughput small-molecule screening and medicinal chemistry expertise for the development of chemical probes for use as tools to explore biological targets or pathways for which small-molecule tools are unavailable (*40*). One such target that lacks the appropriate small-molecule tools is the muscarinic acetylcholine receptors (mAChRs), and in order to understand the relative contributions of M_1 and M_4 to the efficacy of xanomeline, potent and subtype-selective M_1 agonists are required.

High-Throughput Screening and Identification of M_1 Allosteric Agonists

For the discovery of novel allosteric agonists of the M_1 muscarinic receptor, we completed a primary high-throughput (HT) screen using a real-time cell-based assay (Z' averaged 0.7) against the 65 000-member MLPCN compound library. The primary assay was run using CHO cells stably expressing M_1 as described by Marlo et al. (*26*).

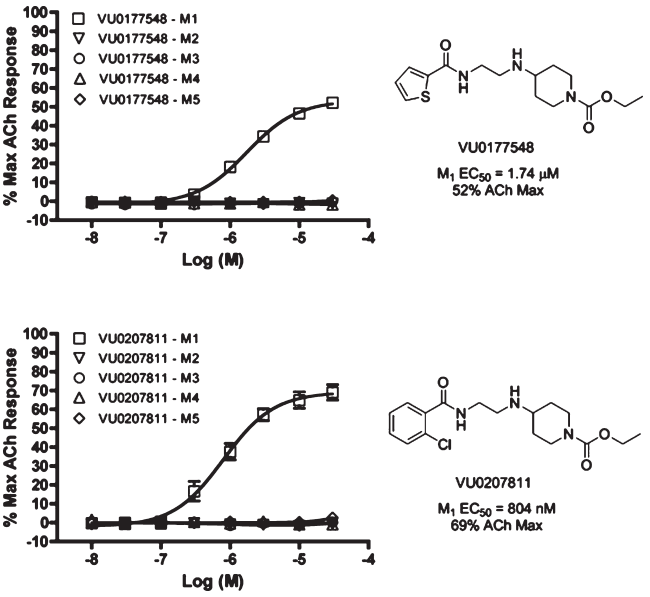

Figure 2. HTS hits VU0177548 and VU0207811 are potent and efficacious M_1 agonists and selective versus M_2−M_5 family members. Concentration−response curves from intracellular calcium mobilization assays show that VU0177548 and VU0207811 exhibit exquisite functional selectivity for the M_1 muscarinic receptor. Notably, no alteration was detected in baseline versus M_2−M_5 subtypes up to the maximal concentration tested, 30 μM.

This effort identified approximately 2000 putative agonist primary hits (*27*). For the confirmation screen, 1666 agonist hits were reordered from Biofocus-DPI. The compounds were tested in duplicate against M_1-CHO cells and, in parallel, counterscreened against M_4/G_{qi5}-CHO cells. Compounds showing initial selectivity for M_1 over M_4 were tested in triplicate in a 10-point concentration−response series against the muscarinic panel (M_1−M_5). Compounds showing selectivity for M_1 were then tested as a concentration series in the presence of atropine. Pubchem CID 644390 and CID 647412 were selective (> 50-fold) for M_1 vs M_4 with M_1 EC_{50}'s from the DPI DMSO stock of ~1 μM and were sensitive to block by atropine. Resynthesis of these hits provided VU0207811 (CID 644390) and VU0177548 (CID 647412) with M_1 EC_{50} values of 804 nM (69% ACh_{max}; ACh_{max} is defined as the maximal observed response following compound dosing normalized to a maximal response elicited by a high concentration of acetylcholine) and 1.74 μM (52% ACh_{max}), respectively, and both displayed high selectivity for M_1 relative to M_2−M_5 (Figure 2). These compounds provided an excellent starting point to initiate a chemical optimization effort aimed at increasing potency and developing properties suitable for studies of selective M_1 activation *in vivo*.

Design, Synthesis and SAR of Analogues of VU0207811

For chemical lead optimization, we employed a diversity-oriented synthesis/iterative screening approach to rapidly

DOI: 10.1021/cn900003h | *ACS Chem. Neurosci.* (2010), *1*, 104–121

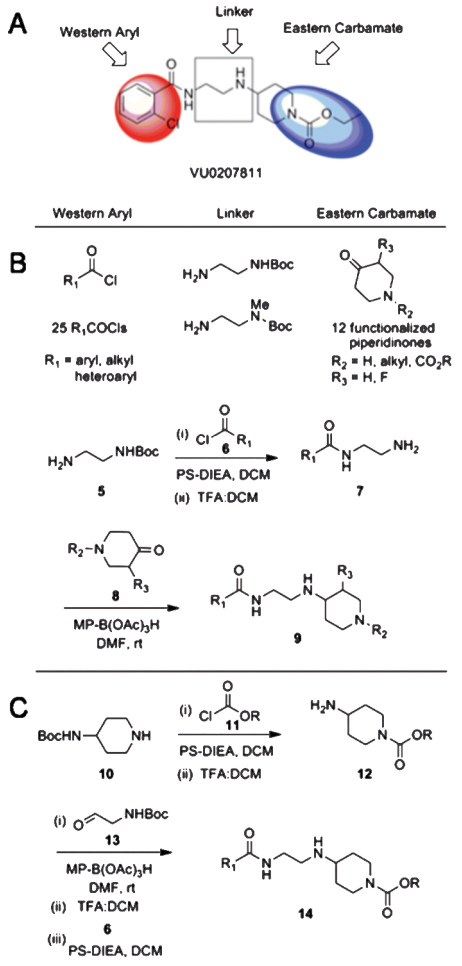

Figure 3. Design and synthetic strategy for chemical lead optimization of VU0207811: (A) diversity-oriented modular design strategy; (B, C) general synthetic approaches employed for iterative library synthesis.

explore structure−activity relationships (SAR), to improve M_1 potency while maintaining selectivity versus M_2−M_5, and to provide an excellent CNS pharmacokinetic profile. We divided the lead compound, VU0207811, into three sections denoted western aryl, linker, and eastern carbamate (Figure 3A). A 25 × 2 × 12 matrix library of analogues was rapidly synthesized, using solution phase parallel synthesis (Figure 3B,C), and subsequently purified by mass-directed preparative HPLC to analytical purity (>98%) (*41*). For example, *N*-Boc-ethylene diamine **5** was acylated with one of 25 acid chlorides **6** to afford, after deprotection, **7**. Reductive amination with a functionalized piperidinone **8** and MP-B(OAc)$_3$H provides analogues **9** in yields averaging 70% for the three-step sequence. Alternatively, 4-*N*-Boc amino piperidine **10** could be treated with diverse chloroformates **11** to afford, after deprotection, **12**. A reductive amination sequence with *N*-Boc *β*-amino-aldehydes **13**, followed by deprotection and acylation with diverse acid chlorides **6**, delivers analogues **14**.

In addition to improvements in potency and efficacy (Figure 4A), shallow SAR was observed for most of the analogues synthesized. Notably, alternate carbamates, *β*-fluorination of the western piperidine ring, and removal of the carboxyl functional group from this moiety abolished M_1 activity (Figure 4B). Thus, even subtle structural changes in this portion of the molecule were not well-tolerated with no improvements made in terms of either potency or efficacy over the initial HTS hits. Unlike the ethyl carbamate moiety, the western aryl was much more amenable to substitution. The ortho, meta and para positions of the phenyl ring could all be readily substituted, with electron-donating groups tolerated ortho and meta and with electron-withdrawing groups tolerated primarily meta and para, but to a limited extent ortho as well. In addition to phenyl substitutions, heterocyclic groups can also be tolerated in this position. The largest gains in potency and efficacy over initial HTS hits were seen with a naked phenyl ring and *o*-methylphenyl ring to yield VU0184670 and VU0357017, respectively. Also, *p*-fluoro (VU0359993), *m*-fluoro (VU0359995) and *m*-methoxy (VU0360014) substitutions were tolerated around the phenyl rings while retaining substantial potency and efficacy (Figure 4A). As lead optimization was being conducted, synthetic libraries were initially screened in parallel in a functional calcium mobilization assay at a single point concentration of 30 μM with CHO-K1 cells stably expressing the rM_1 receptor in order to triage active compounds from inactive compounds. Compounds showing the highest efficacy at 30 μM were then chosen for full eight-point concentration−response curve selectivity profiling across the muscarinic subtypes in the same calcium mobilization assay. This process subsequently yielded the potent and selective candidates VU0184670 and VU0357017. With a potency of 152 nM and ACh_{max} of 85% VU0184670 displays comparable potency and efficacy to the benchmark M_1 allosteric agonist TBPB (**4**).

VU0184670 and VU0357017 Are Selective versus the M_2−M_5 Subtypes and Display No Substantial Ancillary Pharmacology

Within the muscarinic receptors, both VU0184670 and VU0357017 are highly selective for M_1 and had no activity at M_2−M_5 up to the highest concentrations tested (30 μM), as assessed by measuring receptor-mediated increases in mobilization of intracellular calcium (Figure 5A,B). However, demonstration of selective agonist activity at M_1 does not necessarily imply that these compounds are completely inactive at M_2−M_5. It is possible that VU0184670, VU0357017, and related compounds could interact with multiple mAChR subtypes but act as antagonists rather than agonists at other members of this receptor subfamily.

DOI: 10.1021/cn900003h | *ACS Chem. Neurosci.* (2010), *1*, 104–121

A

Cmpd	Structure	M1 EC_{50}	%ACh_{max}
VU0184670	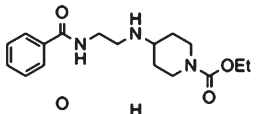	152 nM	85
VU0357017	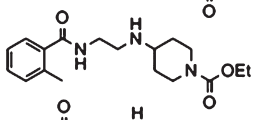	198 nM	81
VU0359993	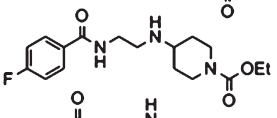	154 nM	79
VU0359995	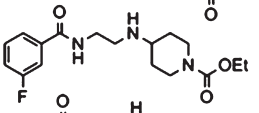	154 nM	72
VU0360014	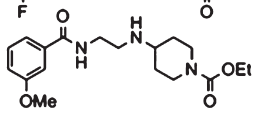	459 nM	80
VU0360010	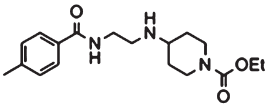	>10 μM	13

B

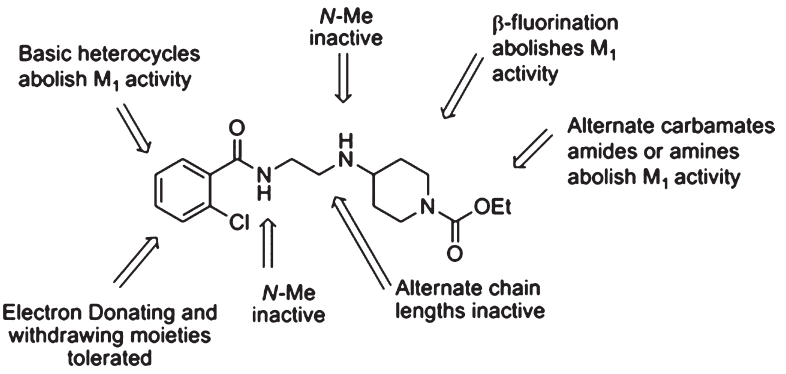

Figure 4. SAR and lead optimization strategy for M_1 allosteric agonists with a diverse subset of analogues derived from initial HTS hits exemplary of observed SAR: (A) diverse subset of synthetic analogues representative of the comprehensive SAR observed during lead optimization showing EC_{50} potency and ACh_{max} efficacy values; (B) summary of observed SAR around VU0184670 showing western aryl and eastern carbamate functional handles.

Thus, we performed additional experiments in which we assessed the abilities of these compounds to inhibit responses to EC_{80} concentrations of ACh at each of the mAChR subtypes. For comparison, we also determined the effects of TBPB, an allosteric M_1 agonist. Interestingly, TBPB inhibited responses to ACh at each of the other mAChR subtypes (Figure 6). While the antagonist activity of TBPB required concentrations that were higher than those for activation of M_1, these data reveal that TBPB is not entirely M_1-selective and has antagonist activity at multiple mAChR subtypes. In contrast, VU0184670, VU0357017, and related analogues had little or no detectable antagonist activity at any other mAChR subtype at concentrations over 2 orders of magnitude higher than those required to activate M_1. In addition, we found that these compounds have an exceptionally clean ancillary pharmacology profile and have no significant activities at concentrations up to 10 μM when assessed in a Panlabs lead profiling screen of 68 GPCRs, ion channels, and transporter targets (Supplementary Table 1, Supporting Information). Importantly, this includes a lack of activity at multiple biogenic amine receptors that has been observed with TBPB as well as the other previously described M_1 agonists (*13*, *21*). Thus, VU0184670 and VU0357017 represent a major breakthrough in providing much more highly selective M_1 agonists than has been achieved with previous allosteric or orthosteric M_1 agonists.

VU0184670 and VU0357017 Are Allosteric Agonists of the M_1 Receptor

The finding that VU0184670 and VU0357017 are highly selective M_1 agonists suggests that these

DOI: 10.1021/cn900003h | *ACS Chem. Neurosci.* (2010), *1*, 104–121

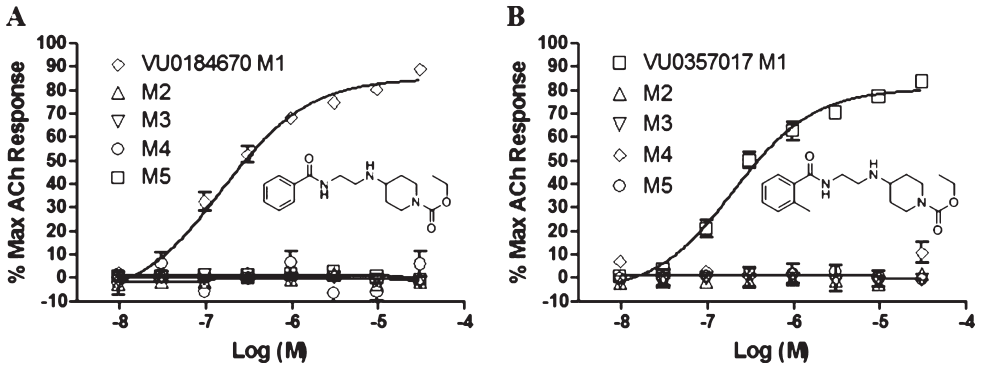

Figure 5. VU0184670 and VU0357017 are potent and efficacious M_1 agonists, selective versus M_2-M_5 family members and allosteric agonists. Concentration−response curves from intracellular calcium mobilization assays: (A) VU0184670 activation of the M_1 receptor is both highly potent and efficacious, with an EC_{50} of 152 ± 8.44 nM and ACh_{max} of 85.01% ± 3.3% max; (B) the high degree of potency, efficacy, and selectivity observed in functional coupling to intracellular calcium release for panel A was reproducible with the close structural analogue, VU0357017, yielding an EC_{50} of 198 ± 13.2 nM and ACh_{max} of 80.52% ± 7.67% max. Importantly, for all analogues tested, no agonism was uncovered at any of the M_2-M_5 subtypes up to the maximal 30 μM assay concentration. Results are from three independent experiments ± SEM.

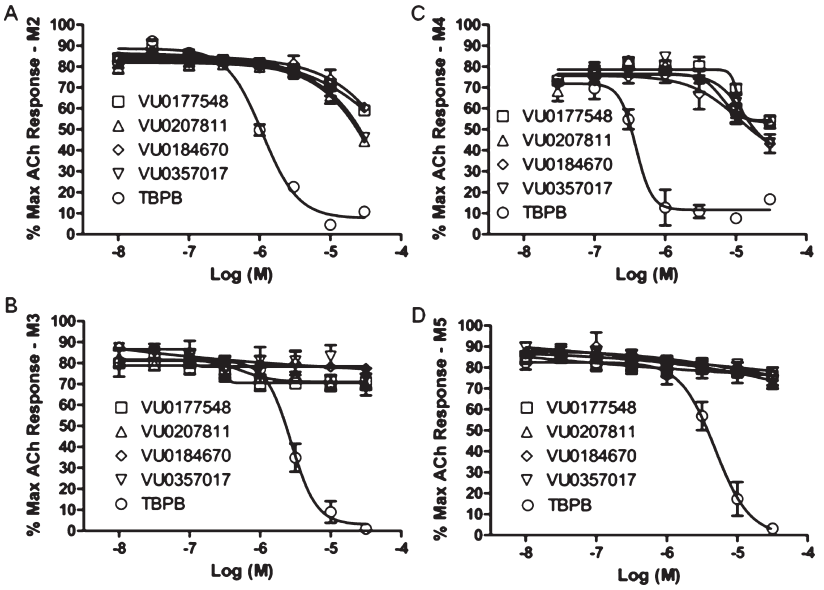

Figure 6. Antagonism profile for novel M_1 allosteric agonists and M_1 allosteric agonist TBPB versus M_2-M_5. Dose−response curves showing the ability of novel M_1 agonists to attenuate an EC_{80} response of ACh in order to evaluate functional selectivity in terms of antagonism at M_2-M_5 receptor subtypes: (A) antagonism selectivity at M_2 receptor subtype was found to be > 30 μM for all novel agonists tested, with benchmark allosteric agonist TBPB giving a IC_{50} of 1.1 μM ± 0.169 μM; (B) all novel agonists demonstrated > 30 μM selectivity for M_3, while TBPB was found to have an IC_{50} of 3.0 μM; (C) when assayed for selectivity at M_4, again all novel agonists showed > 30 μM selectivity, while TBPB showed potent antagonism yielding an IC_{50} of 415 ± 165 nM; (D) all novel agonists demonstrated > 30 μM selectivity at the M_5 subtype, with TBPB giving an IC_{50} of 10.1 μM. Results are from three independent experiments; error bars indicate ±SEM.

compounds are unlikely to act at the highly conserved orthosteric site on M_1 and are more likely to act as allosteric agonists. We performed a series of studies aimed at testing this hypothesis. First, we determined the effects of these compounds on a mutant form of M_1 that bears a single point mutation (M_1 Y381A) previously shown to dramatically reduce the affinities of ACh and other orthosteric ligands (Figure 7). Previous studies suggest that NDMC, AC42, TBPB, and other allosteric agonists activate M_1Y381A with potencies similar to their potencies at the WT receptor, whereas the potencies of ACh and carbachol, orthosteric agonists, are dramatically reduced (*16*, *26*, *39*). Consistent with previous reports, the potency of ACh was found to be dramatically reduced in M_1 Y381A CHO cells, whereas the allosteric agonist NDMC induced a robust response with a potency similar to that observed in cells expressing WT M_1 (data not shown) (*16*, *26*, *39*). In contrast to the rightward shift observed with orthosteric agonists, VU0184670, VU0357017, and related compounds induced robust increases in calcium mobilization in M_1 Y381A CHO cells with potencies similar to

DOI: 10.1021/cn900003h | *ACS Chem. Neurosci.* (2010), *1*, 104–121

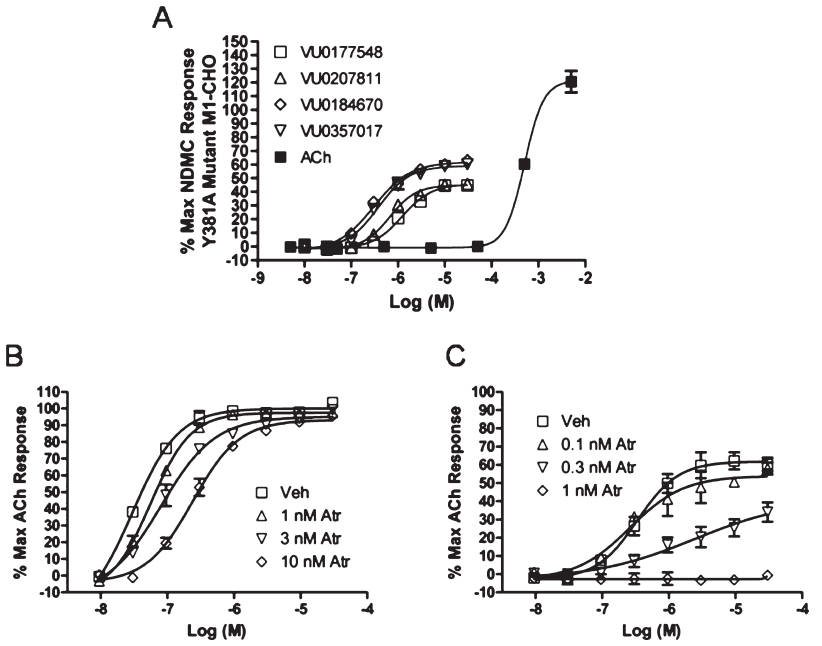

Figure 7. New M_1 agonists activate M_1 via an allosteric site. (A) VU0184670 and related novel agonists were found to elicit a functional response comparable to that on wt rM_1 cells when dosed on rM_1 Y381A cells bearing an orthosteric mutation that ablates orthosteric agonist binding. Agonist-evoked responses for VU0184670 showed an EC_{50} of 304 ± 156 nM and ACh_{max} of 63.25% ± 1.5% max and those for VU0357017 an EC_{50} of 379 ± 912 nM. Initial hits VU0177548 and VU0207811 displayed EC_{50} values and maximal efficacies of 1.23 ± 0.23 μM and 44.69% ± 4.90% max and 660 ± 115 nM and 45.80% ± 5.45% max, respectively. The concentration−response curve for orthosteric ACh is substantially right-shifted from that observed with WT rM_1 cells. Results are from three independent experiments ± SEM. (B) Schild analysis showing a concentration−response curve of carbachol applied to rM_1 cells in the presence of fixed, increasing concentrations of the orthosteric muscarinic antagonist atropine. A parallel rightward shift in the concentration−response curve for carbachol was observed, consistent with carbachol being an orthosteric agonist and competing with atropine for binding to the orthosteric site. (C) Schild analysis showing a concentration−response curve of VU0184670 applied to rM_1 cells in the presence of fixed, increasing concentrations of the orthosteric muscarinic antagonist atropine. A rightward shift with diminished efficacy was observed in the VU0184670 concentration−response curve with increasing concentrations of atropine, consistent with noncompetitive antagonism and VU0184670 having an allosteric mechanism of action at the M_1 receptor. Results are from three independent experiments; error bars represent ±SEM.

those observed in WT M_1 CHO cells (Figure 7A). The finding that a mutation known to reduce affinities of orthosteric ligands was without effect on responses to these novel M_1 agonists is consistent with the hypothesis that these compounds act at an allosteric site to activate M_1.

If these M_1 agonists activate the receptor by acting at an allosteric site, they should not interact in a competitive manner with an orthosteric M_1 antagonist. Thus, to further test the hypothesis that VU0184670 is an allosteric agonist of M_1, we performed a Schild analysis to determine the effects of the orthosteric antagonist atropine on the concentration response relationships of VU0184670 and ACh. Consistent with the known mechanism of action of atropine as an orthosteric site antagonist, atropine induced parallel rightward shifts of the ACh concentration−response relationship (Figure 7B), suggesting that atropine and ACh interact in a purely competitive manner. In contrast, increasing concentrations of atropine induced progressive downward shifts in the concentration−response relationship of VU0184670, reducing the maximal response that could be achieved with this novel agonist (Figure 7C). These data provide strong evidence that atropine blocks the response to VU0184670 in a noncompetitive manner suggesting that these compounds do not interact at the same site. These data provide further support for the hypothesis that VU0184670 activates M_1 by acting at an allosteric site.

We next performed competition binding experiments as a final measure to directly determine whether VU0184670 binds to the orthosteric site in a competitive manner. Orthosteric site binding was assessed by measuring the ability of increasing concentrations of VU0184670 to displace binding of the orthosteric radioligand [^{3}H]-*N*-methylscopolamine ([^{3}H]-NMS) (Figure 8). Interestingly, VU0184670 and related analogues did not reduce [^{3}H]-NMS binding to the M_1−M_5 muscarinic receptors at concentrations well above those required to fully activate M_1, further implicating an allosteric mechanism of action. In contrast, the orthosteric antagonist atropine competes with [^{3}H]-NMS for binding to all muscarinic subtypes with a potency consistent with its high affinities at the mAChR subtypes. Taken together, these data provide compelling evidence that VU0184670 and analogues in this series act via an allosteric mechanism in order to activate M_1.

DOI: 10.1021/cn900003h | *ACS Chem. Neurosci.* (2010), *1*, 104–121

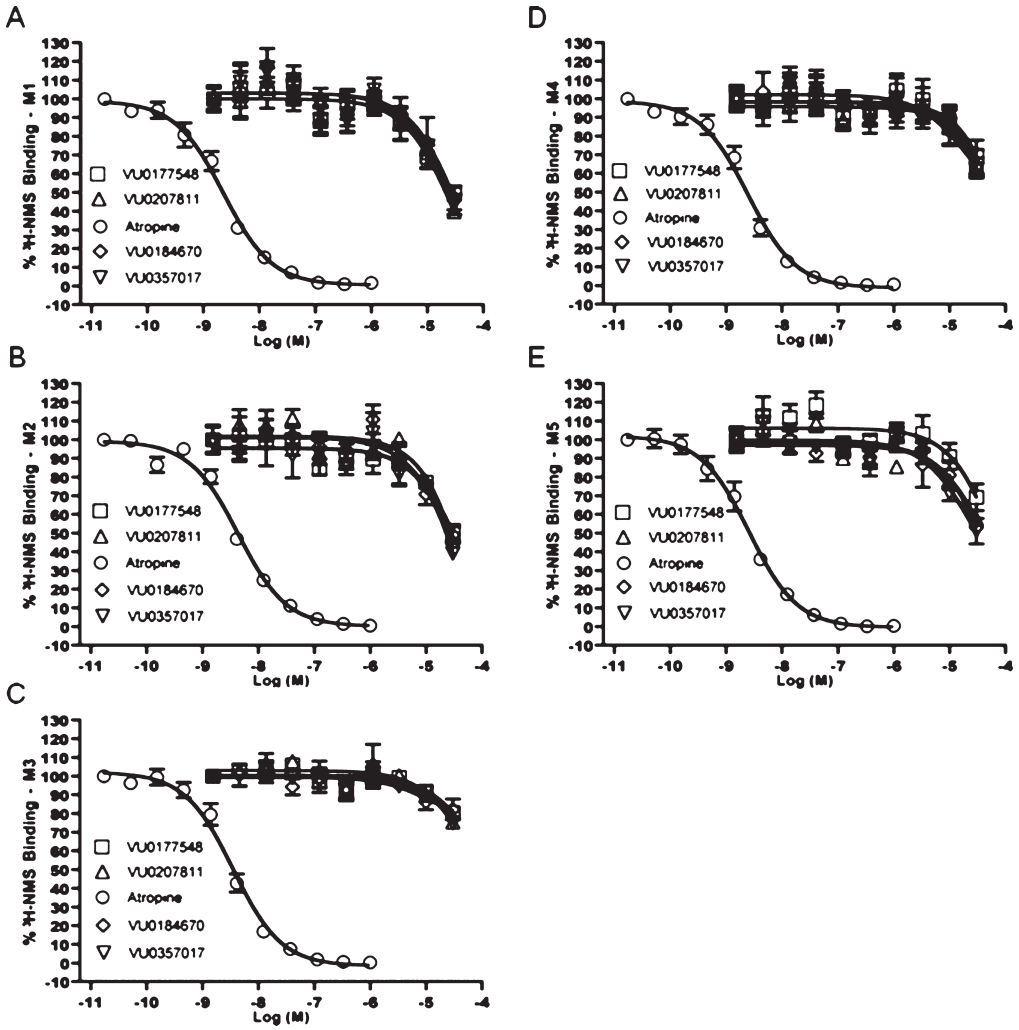

Figure 8. VU0184670 and related analogues do not compete with [^{3}H]-NMS for binding to the M_1 receptor, further consistent with a mode of allosteric agonism. [^{3}H]-NMS competition binding for novel allosteric agonists reveal that all possess IC_{50} values $> 30\,\mu M$ and do not appear to compete with the orthosteric [^{3}H]-NMS, which further corroborates these agonists binding to the M_1 receptor via an allosteric mechanism of action (A−E). For atropine controls at individual subtypes, (A) atropine was found to have an M_1 IC_{50} of 2.22 ± 0.60 nM and K_i of 1.27 ± 0.36 nM, (B) M_2 atropine $IC_{50} = 4.32 \pm 1.63$ nM and $K_i = 3.24 \pm 1.16$ nM, (C) M_3 atropine $IC_{50} = 4.16 \pm 1.04$ nM and $K_i = 2.21 \pm 0.53$ nM, (D) M_4 atropine $IC_{50} = 2.38 \pm 1.07$ nM; $K_i = 0.77 \pm 0.34$ nM, and (E) M_5 atropine $IC_{50} = 3.39 \pm 1.16$ nM and $K_i = 2.84 \pm 0.84$ nM. Results are from three independent experiments; error bars represent ±SEM.

Mutations of E401 and E397 Reduce VU0184670-Induced Activation of the M_1 Receptor

In order to further characterize the binding mode of VU0184670 at the M_1 receptor, site-directed mutagenesis was undertaken in parallel with a hypothesis-driven molecular modeling approach to deduce residues that might mediate ligand-induced receptor activation. A triple mutant pcDNA3.1$^+$ vector containing a WT rat cDNA bearing K392D, E397V, and E401H mutations was constructed and transiently transfected into CHO cells, with functional activation of the receptor monitored by intracellular calcium mobilization. These residues are located in extracellular loop three (ECL3) and the first helical turn of transmembrane seven (TM7) of the M_1 receptor. Previous studies suggest that this region is important for the actions of some other allosteric ligands of the M_1 receptor (*29*−*32*). Interestingly, introduction of a triple mutation of residues K392D, E397V, and E401H almost completely ablated the functional response of M_1 to VU0184670. Based on the location of these residues in M_1, the effects of these mutations implicate ECL3 and the first helical turn of TM7 as important for mediating the observed agonist activity of VU0184670 at the M_1 receptor (Figure 9). Molecular models were generated for the M_1 receptor based on the X-ray structure of the β2 adrenergic receptor (PDB ID 2RH1) for the purpose of hypothesis generation to assess potential binding sites for interaction with VU0184670 (unpublished findings). Flexible

DOI: 10.1021/cn900003h | *ACS Chem. Neurosci.* (2010), *1*, 104–121

A	wt rM_1		K392D/E397V/E401H		EE397/401DD		K392D		E397V	
	EC_{50}	ACh_{max}	EC_{50}	ACh_{max}	EC_{50}	ACh_{max}	EC_{50}	ACh_{max}	EC_{50}	ACh_{max}
VU0184670	97.9 nM ± 0.693 nM	56.55 % ± 5.22 % max	8.92 μM ± 1.90 μM	11.13 % ± 0.84 % max	2.87 μM ± 5.72 μM	24.33 % ± 2.11 % max	108.3 nM ± 7.71 nM	46.29 % ± 9.19 % max	152.7 nM ± 52.8 nM	34.31 % ± 1.70 % max
	E397D		E401H		E401A		E401D			
	EC_{50}	ACh_{max}	EC_{50}	ACh_{max}	EC_{50}	ACh_{max}	EC_{50}	ACh_{max}		
	174.3 nM ± 52.8 nM	42.56 % ± 4.00 % max	1.21 μM ± 83.4 nM	29.44 % ± 4.16 % max	788.8 nM ± 29.8 nM	29.35 % ± 3.16 % max	1.25 μM ± 646.6 nM	24.58 % ± 3.91 % max		

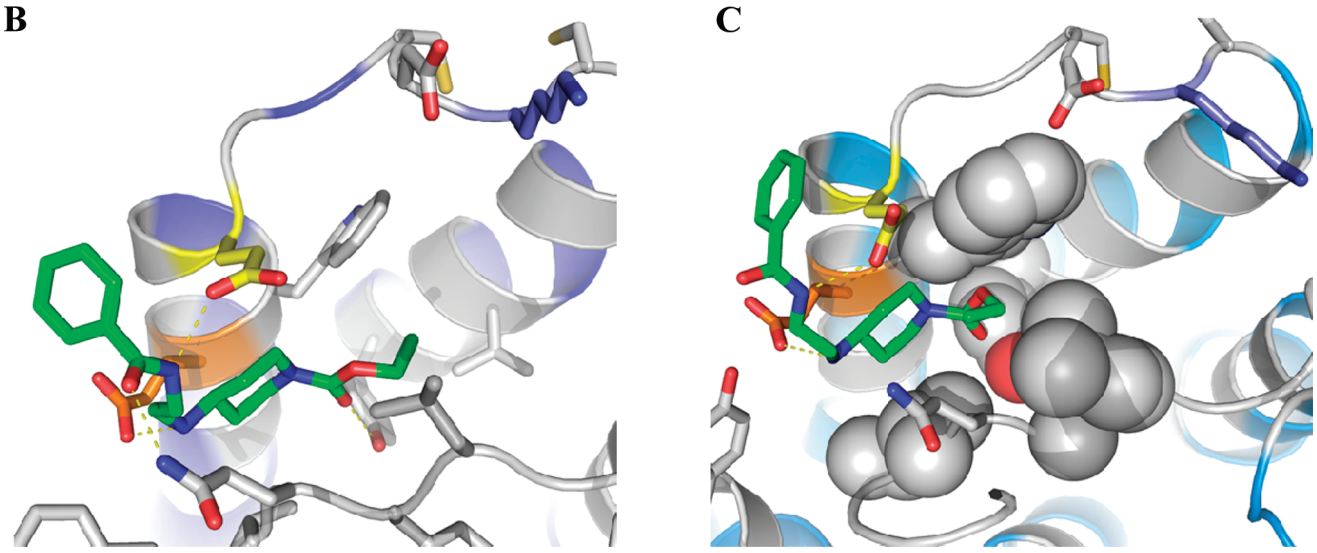

Figure 9. Extracellular loop 3 and the first helical turn of transmembrane seven are involved in mediating the binding of VU0184670 to the M_1 receptor. (A) Site-directed mutagenesis data showing targeted mutagenesis effort of amino acid residues in the third extracellular loop and first turn of the seventh transmembrane span of the M_1 receptor. When a dose−response curve was constructed for novel agonists tested in a functional calcium mobilization assay on transiently transfected K392D/E397V/E401H triple-, EE397/401DD double-, and related E401 single-point mutant CHO-K1 cells, functional potency was nearly completely lost for VU0184670. Not much potency appeared to be lost when increasing concentrations of agonist were applied on cells bearing K392D, E397V, or E397D single mutations, but the E401H single mutation led to substantial losses in potency for both VU0184670 (EC_{50} = 1.21 μM; E_{max} = 29.4%) when compared with WT. Additionally, E401A and E401D mutations resulted in similar losses in potency. (B) Automated flexible ligand docking of VU0184670 (green) into a homology model of the M_1 receptor (blue ribbon) based on the X-ray crystal structure of the β2 adrenergic receptor (PDB ID 2RH1). Gradient energy-minimized models illustrated physically plausible low-energy complexes with potential to form up to four hydrogen bonds (dashed yellow lines) with E401 (orange), E397 (yellow), Y381, and Q181. (C) Complexes of VU0184670 allosteric agonist with the M_1 receptor (shown) were among the top 10 scoring docking poses (of 5000 models generated), were consistent with pronounced and graded effects from mutagenesis of E401/E397, and generally agree with ligand SAR profiles by placing the western aryl moiety toward extracellular space and the eastern ethyl carbamate moiety into a buried, sterically occluded region of the receptor extracellular binding domain involving I180, F182, L183, Y381(located beneath VU0184670), and W400 (space-filling representations). Results are for three independent experiments with errors given as ±SEM.

ligand docking of VU0184670 (with an initial placement of the ligand into the ECL3/TM7 region as described above; see Methods) identified 10 distinct binding poses with two large clusters representing ~40% of the best scoring 1000 structures. Representative structures from each cluster were examined by visual inspection for protein−ligand interactions consistent with the loss of function observed in the K392D/E397V/E401H triple mutant. The second largest cluster (representing ~10−12% of the best 1000 models) contained two models from the top 10 overall protein−ligand interface scores (Figure 9B,C). These two binding poses formed up to four protein−ligand hydrogen bonds with E401, E397, Q181, or Y381 side chains and an intermolecular ion−pair interaction with the E401 side chain and were in general agreement with the comprehensive SAR observed with all analogues synthesized. As one can see from these agonist-docked models, the positioning of the linear diamine scaffold of VU0184670 within the ECL3/TM7 region places the secondary amine of the backbone in close proximity to E401. Since this secondary amine will be charged at physiological pH, a salt bridge contact formed between E401 and this backbone amine could help to explain the observed potency of

DOI: 10.1021/cn900003h | ACS Chem. Neurosci. (2010), 1, 104–121

VU0184670. In addition to this contact, the relative eastern versus western orientation of the agonist-docked molecule is such that the eastern carbamate moiety points down toward the orthosteric binding site while the western aryl group points more toward the solvent front. This could help to explain the SAR observed with VU0184670 because the contributing residues (I180, Q181, F182, L183, Y381, W400) from the upper two helical turns and second extracellular loop (ECL2) in this binding pose contact the eastern portion of the agonist to produce a region that is much more sterically occluded than the western counterpart (Figure 9C). Thus, the substantial steric occlusion that results in burial of the eastern carbamate moiety toward the orthosteric site may help to explain why slight structural changes introduced into the eastern portion of the molecule during lead optimization were not well-tolerated. Conversely, the solvent accessibility of the western aryl group of VU0184670 (oriented toward the extracellular space above TM7) may help to explain why this moiety displayed less-stringent SAR and could be much more readily substituted (Figure 9C).

In order to deduce contributions to agonist activity on an individual basis, the same wt rM_1 cDNA was used to construct vectors bearing the corresponding single mutations, K392D, E397V, and E401H (Supplementary Figure 1, Supporting Information). When assessed for functional activity, K392D appeared to yield comparable results to WT rM_1, precluding it as a critical residue for mediating the observed agonist activity of VU0184670. The E397V mutation yielded a mild reduction in potency and efficacy, whereas E401H substantially decreased both potency and efficacy of VU0184670 to a degree that much more closely approximated the K392D/E397V/E401H mutant (Supplementary Figure 1, Supporting Information). In order to preserve the native charge of the glutamate residues and to test the contribution of side-chain length to potential interactions with the allosteric agonist, single point mutations of E397D, E401D, and E401A were generated based on visual inspection of an M_1 model with manually docked VU0184670 to further test and support the role of the acidic residues at E397/E401 in M_1 receptor binding of VU0184670. All of these experiments yielded Ca^{2+} fluorescence traces in agreement with those observed for the E397V and E401H mutations. Finally, in an attempt to fully recapitulate the result observed with the initial triple mutant by perturbing a putative binding mode posited from our docked models of M_1 with VU0184670, an EE397/401DD double mutant was generated that did in fact appear to decrease the potency and efficacy further toward the levels observed with the triple mutant.

VU0184670 Potentiates NMDAR Current

Discovery of highly selective M_1 receptor allosteric agonists provides an exciting new tool to probe the effects of selective activation of the M_1 receptor in CNS preparations and in vivo. One of the most well-established physiological effects of M_1 receptor in the CNS is potentiation of currents through the *N*-methyl-D-aspartate subtype of glutamate receptor (NMDAR) (*15*, *20*). Modulation of the NMDAR currents by M_1 has been postulated to play a critical role in cholinergic regulation of cognitive function and in regulation of brain circuits that are thought to be critical for the efficacy of mAChR agonists in both AD and schizophrenia (*15*−*18*). Based on this, we performed studies using whole-cell patch clamp recordings from hippocampal CA1 pyramidal cells to test the hypothesis that selective activation of the M_1 receptor with VU0184670 would potentiate NMDAR current in these cells. Pressure ejection of NMDA (1 mM) produced a stable inward current in CA1 pyramidal cells voltage-clamped at −60 mV. Bath application of VU0184670 (30 μM) produced an increase in the peak amplitude of NMDA-evoked currents in CA1 pyramidal cells (Figure 10A,B). The increased amplitude of NMDAR currents induced by VU0184670 peaked at 137.5% ± 11.3% of baseline (n = 6, p = 0.021) approximately 2 min after initial application of VU0184670. These data suggest that VU0184670 elicits a well-characterized response to M_1 receptor activation in native systems that is thought to play an important role in mAChR regulation of synaptic plasticity and cognitive function.

VU0184670 and VU0357017 are CNS Penetrant

With regard to physiochemical properties, all compounds produced from this lead optimization effort were very attractive, because they are all extremely water-soluble small molecules (>25 mg/mL in saline as mono-HCl salt), rendering them very promising in terms of both basic science applications and leads for potential therapeutic agents. For compounds to have utility in the CNS *in vivo* or to be useful for therapeutic applications, it is imperative that the compounds cross the blood−brain barrier to achieve *in vivo* central penetrance. Thus, we performed studies in which we measured the levels of VU0184670 and VU0357017 in rat plasma and brain at various time points after ip administration. VU0184670 and VU0357017 were both found to be centrally penetrant (Supplementary Figure 2, Supporting Information). While both compounds displayed central penetrance, VU0357017 was more readily cleared from the CNS than VU0184670 and displayed superior pharmacokinetic properties with a log BB of 1.46 and a 4:1 brain/plasma ratio (4338.90 ± 1071.20 ng/mL to 1053.49 ± 276.03 ng/mL). VU0184670 on the other hand was not as readily cleared as VU0357017,

DOI: 10.1021/cn900003h | *ACS Chem. Neurosci.* (2010), *1*, 104–121

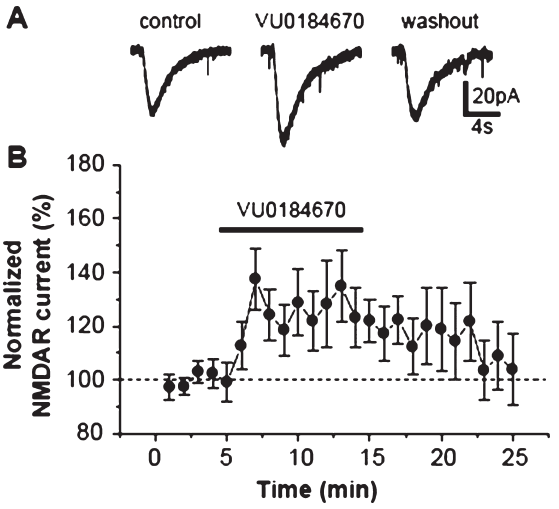

Figure 10. VU0184670 potentiates NMDAR currents in CA1 pyramidal cells. Representative whole cell traces of NMDA-evoked currents obtained from a typical experiment (A) and time course of normalized amplitude of NMDAR currents before, during, and after application of 30 μM VU0184670 to rat hippocampal slices (n = 6) (B). Notably, even following washout, the potentiation appeared to persist for almost 10 min. Error bars represent mean ± SEM for six independent experiments.

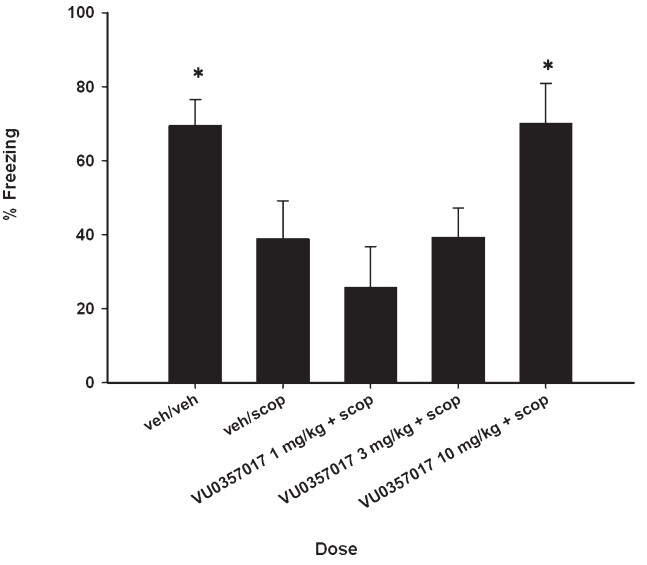

Figure 11. VU0357017 reverses scopolamine-induced disruption of the contextual fear conditioning response. Scopolamine (0.2 mg/kg, sc) produced a robust disruption in the acquisition of contextual fear conditioning response as shown by a decrease in the percent of time spent freezing in the same context environment as the training session. At a dose of 10 mg/kg (ip), VU0357017 produced a significant reversal of the scopolamine-induced disruption of the contextual fear conditioning response by Dunnett's comparison with vehicle/scopolamine-treated group. Results are expressed as mean percent freezing behavior ± SEM (n = 3−4 rats per treatment group). The ∗ indicates $p < 0.05$ when compared with the vehicle/scopolamine group.

appearing to sequester within the CNS with increasing concentrations over time to yield a brain/plasma ratio of 14490.12 ± 2663.82 ng/mL to 311.86 ± 20.77 ng/mL. The high aqueous solubility (>25 mg/mL in H_2O) and pharmacokinetic parameters, coupled with the fact that VU0357017 is readily centrally penetrant and displays a favorable ancillary pharmacological profile suggest that this compound could provide an excellent tool for studies of the effects of M_1 receptor activation *in vivo*.

VU0357017 Is Active in Reversing Cognitive Deficits in a Preclinical Rodent Model When Dosed Systemically

We next evaluated the ability of VU0357017 to reverse cognitive deficits induced by the orthosteric mAChR antagonist scopolamine in a contextual fear conditioning paradigm. Importantly, this task is a model of hippocampal memory, and M_1 is highly expressed in the hippocampus. In this paradigm, rats first undergo a training period in which an unconditioned aversive stimulus (US), such as a mild footshock that elicits a freezing behavior, is paired with a neutral conditioned stimulus (CS), in this case the environment or context. The following day, during the testing period, exposure to the testing environment or context (CS) alone can elicit a freezing behavior, also known as the contextual fear conditioning response. The nonselective muscarinic antagonist scopolamine, administered (0.2 mg/kg sc) 15 min prior to the training period, produced a significant disruption in the acquisition of the contextual fear conditioning response. VU0357017, at a dose of 10 mg/kg ip, produced a significant reversal of the scopolamine-induced deficits ($p < 0.05$, ANOVA, Dunnett test) in the acquisition of this behavior (Figure 11).

In summary, using a functional HTS and subsequent diversity-oriented synthesis approach, we have discovered a novel series of highly selective, centrally penetrant M_1 allosteric agonists. Detailed *in vitro* molecular pharmacology studies indicated that they are indeed allosteric agonists. Moreover, mutagenesis studies demonstrated that this series of M_1 allosteric agonists, typified by VU0184670 and VU0357017, bind at a novel allosteric site in the third extracellular loop of the M_1 mAChR. As a result, these new M_1 allosteric agonists displayed unprecedented selectivity versus M_2−M_5 and a large panel of GPCRs, ion channels, and transporters. Representative analogues potentiated NMDAR currents and reversed scopolamine-induced disruption of the contextual fear conditioning response *in vivo*. VU0357017 represents the most advanced and selective small molecule tool known to selectively study M_1 receptor activation *in vitro* and *in vivo* and can serve as a viable lead for discovery efforts aimed at developing novel therapeutic agents to treat Alzheimer's disease and schizophrenia. (VU0357017 is an MLSCN probe available for free; use the identifier CID25010775 (*40*)).

DOI: 10.1021/cn900003h | *ACS Chem. Neurosci.* (2010), *1*, 104–121

Methods

Chemical Synthesis and Purification

Synthesis of VU0184670 (1): Ethyl 4-(2-Benzamidoethylamino)piperidine-1-carboxylate. To a solution of benzoyl chloride (87.7 mg, 0.624 mmol) in dichloromethane (2 mL) was added *N*-boc-ethylenediamine (100.0 mg, 0.624 mmol) and PS-DIEA (2 equiv, 356.6 mg). The reaction was agitated overnight at room temperature, after which the reaction mixture was filtered to remove polymer-supported resin. The filtrate was then concentrated and dissolved in 1 mL of dichloromethane, to which was added 1 mL of trifluoroacetic acid (1:1 DCM/TFA), and the mixture was stirred at room temperature for 30 min. Following deprotection, the reaction mixture was again concentrated to dryness, after which the product was dissolved in dimethylformamide (2 mL). To this solution was added 1-carbethoxy-4-piperidone (106.8 mg, 0.624 mmol) and MP-BH(OAc)$_3$ (2.5 equiv, 645 mg). The reaction mixture was then agitated overnight at room temperature, after which the resin was filtered off. Aqueous workup of the reaction mixture using brine and ethyl acetate, followed by filtration of the organic layer using an Isolute phase separator and sample concentration, yielded ethyl 4-(2-(2-methylbenzamido)ethylamino)piperidine-1-carboxylate as a pale yellow oil. The product was then dissolved in 1 mL of DMSO and purified by mass-directed preparative HPLC to afford ethyl 4-(2-(2-methylbenzamido)ethylamino)piperidine-1-carboxylate-2,2,2-trifluoroacetate as a clear oil (64.5 mg, 23.9%); ^{1}H-NMR (400 MHz, d_6-DMSO) δ 7.9−7.8 (m, 1H), 7.52−7.42 (m, 5H), 6.73 (br s, 1H), 4.16−4.11 (q, J = 7.07 Hz, 1H), 3.56−3.50 (m, 4H), 2.92−2.90 (m, 6H), 2.29 (s, 1H), 1.38−1.32 (m, 7H); ^{13}C NMR (100 MHz, d_6-CDCl$_3$) δ 166.95, 154.84, 134.20, 131.82, 128.65, 127.78, 61.24, 54.36, 43.60, 42.03, 36.30, 14.95; HRMS (*m*/*z*) [M + H] calcd for $C_{17}H_{26}N_3O_3$, 320.1974; found, 320.1966.

Synthesis of VU0357017: Ethyl 4-(2-(2-Methylbenzamido)ethylamino)piperidine-1-carboxylate. To a solution of *o*-toluoyl chloride (96.5 mg, 0.624 mmol) in dichloromethane (2 mL) was added *N*-boc-ethylenediamine (100.0 mg, 0.624 mmol) and PS-DIEA (2 equiv, 356.6 mg). The reaction was agitated overnight at room temperature, after which the reaction mixture was filtered to remove polymer-supported resin. The filtrate was then concentrated and dissolved in 1 mL of dichloromethane, to which was added 1 mL of trifluoroacetic acid (1:1 DCM/TFA), and the mixture was stirred at room temperature for 30 min. Following deprotection, the reaction mixture was again concentrated to dryness, after which the product was dissolved in dimethylformamide (2 mL). To this solution was added 1-carbethoxy-4-piperidone (106.8 mg, 0.624 mmol) and MP-BH(OAc)$_3$ (2.5 equiv, 645 mg). The reaction mixture was then agitated overnight at room temperature, after which the resin was filtered off. Aqueous workup of the reaction mixture using brine and ethyl acetate, followed by filtration of the organic layer using an Isolute phase separator and sample concentration, yielded ethyl 4-(2-(2-methylbenzamido)ethylamino)piperidine-1-carboxylate as a pale yellow oil. The product was then dissolved in 1 mL of DMSO and purified by mass-directed preparative HPLC to afford ethyl 4-(2-(2-methylbenzamido)ethylamino)piperidine-1-carboxylate-2,2,2-trifluoroacetate as a clear oil (102.9 mg, 36.9%); ^{1}H NMR (400 MHz, d_6-CDCl$_3$) δ 7.37−7.18 (m, 7H), 6.30 (br s, 1H), 4.15−4.10 (q, J = 7.07 Hz, 1H), 3.54−3.50 (q, J = 5.74 Hz, 4H), 2.91−2.86 (m, 6H), 2.35 (s, 1H), 1.27−1.20 (m, 7H); ^{13}C NMR (100 MHz, d_6-DMSO) δ 130.96, 129.99, 127.76, 125.83, 61.23, 54.32, 43.38, 42.01, 28.07, 20.01, 14.94; HRMS (*m*/*z*) [M + H] calcd for $C_{18}H_{28}N_3O_3$, 334.2131; found, 334.2130.

Primary High-Throughput Screening

Rat M$_1$-CHO cells (10 000 cells/20 μL/well) were plated in black-walled, clear-bottomed, tissue culture-treated, 384-well plates (Greiner Bio-One, Monroe, NC) in Ham's F-12 medium with 10% FBS and 20 mM HEPES. The cells were grown overnight at 37 °C in the presence of 5% CO_2. The next day, the medium was removed using a VSpin (Velocity 11; Agilent Technologies, Santa Clara, CA) fitted with a modified bucket allowing the 384-well plate to be mounted inverted over a catch basin and spun at 80*g* for 10 s with 40% acceleration and deceleration.

The medium was replaced, using a Combi (Thermo Fisher Scientific, Waltham, MA), with 20 μL of 2 μM Fluo-4/acetoxymethyl ester (Invitrogen) for 45 min at 37 °C. Fluo-4/acetoxymethyl ester was prepared as a 2.3 mM stock in DMSO, mixed in a 1:1 ratio with 10% (w/v) Pluronic acid F-127, and diluted in assay buffer (Hanks' balanced salt solution (HBSS), 20 mM HEPES, and 2.5 mM probenecid; Sigma-Aldrich, St. Louis, MO). Dye solution was removed using the VSpin and replaced with 20 μL of assay buffer using a Combi. Test compounds were transferred to daughter plates using an Echo acoustic plate reformatter (Labcyte, Sunnyvale, CA) and then diluted into assay buffer, using a Combi, to generate a 20 μM stock. Ca^{2+} flux was measured using the Functional Drug Screening System 6000 (FDSS6000; Hamamatsu, Tokyo, Japan). Baseline readings were taken (10 images at 1 Hz; excitation, 470 ± 20 nm; emission, 540 ± 30 nm), and then test compounds (20 μL/well) were added using the FDSS6000's integrated pipettor. For the primary screen, test compounds were applied to cells (final concentration, 10 μM) at 19 s into the protocol, and agonist response was measured as a maximal increase in fluorescence over baseline. The overall assay protocol was automated using the instruments noted above integrated with a robotic arm (F3; Thermo Fisher Scientific) under the control of a Polara scheduler (Thermo Fisher Scientific). All data were recorded to instrument local drives and later migrated to a network drive. FDSS6000 data were analyzed using a custom analysis application and were associated with unique compound identifiers based on liquid handler transfer logs and plate barcode readings captured by the Echo and by Polara. "Hits" were selected by comparing the amplitude of maximal agonist responses as fluorescence over basal following test compound application.

Calcium Mobilization Assays

For measurement of agonist-evoked increases in intracellular calcium, CHO-K1 cells stably expressing muscarinic receptors were plated in 100 μL of growth medium at 5×10^4 (rM1, hM3, and hM5) or 6×10^4 cells per well (rM1 Y381A, hM2/Gqi5, and rM4/Gqi5) in Costar 96-well black-walled,

DOI: 10.1021/cn900003h | ACS Chem. Neurosci. (2010), 1, 104–121

tissue culture (TC)-treated, clear bottom plates (Fisher). Cells were incubated overnight at 37 °C in 5% CO_2. The next day, medium was removed from the cells, and they were incubated with 50 μL of 2 μM Fluo-4 AM diluted in assay buffer [HBSS (Invitrogen) supplemented with 20 mM HEPES and 2.5 mM probenecid, pH 7.4] for 1 h at 37 °C. Dye was removed and replaced with 45 μL of assay buffer. Agonists were diluted into assay buffer at a 2× concentration, and 45 μL was applied to cells using the automated system at 19 s into the 130 s protocol. Calcium flux was measured over time as an increase in fluorescence (fold over basal) using the Flexstation plate reader (Molecular Devices).

Plasma−Brain Exposure Profile PK Study

VU0357017 and VU0184670 were dissolved in sterile water at a concentration of 5 mg/mL (base form) and administered intraperitoneally to male Sprague−Dawley rats weighing 225−250 g (Harlan Sprague−Dawley, Inc., Indianapolis, IN) at a dose of 10 mg/kg. The rat blood and brain were collected at 0.5, 1, 2, 4, and 8 h. Animals were euthanized and decapitated, and the brains were removed, thoroughly washed with cold phosphate-buffered saline, and immediately frozen on dry ice. Trunk blood was collected in EDTA Vacutainer tubes, and plasma was separated by centrifugation and stored at −80 °C until analysis. Three animals were used for each time point.

On the day of analysis, frozen whole rat brains were weighed and homogenized in 1:3 (w/w) volumes of ice-cold phosphate-buffered saline (pH 7.4). The sample extraction of plasma (100 μL) and brain homogenate (250 μL) was performed by a method based on protein precipitation, using 3 volumes of cold acetonitrile containing 0.1% formic acid and an internal standard (VU-178) having final concentration of 50 ng/mL. Extracts were vortex mixed for 5 min followed by centrifugation at 14 000 rpm for 10 min.

The supernatants of plasma and brain homogenate extracts were analyzed by means of HPLC/MS/MS, using a ThermoFinnigan TSQ Quantum Access (Thermo Fisher Scientific, Waltham, MA) mass spectrometer in positive ion mode. The chromatographic separation was achieved on an Acquity UPLC BEH C18 column (1.7um; 2.1 × 50 mm^2) at a flow rate of 0.8 mL/min. The gradient program was used with the mobile phase, combining solvent A (95:5:0.1% formic acid in water/acetonitrile) and solvent B (95:5:0.1% formic acid in water/acetonitrile) as follows: 20% B for 0−0.5 min, 20−95% B for 0.5−1 min, 95% B for 1−2 min, 95−20% B for 2−2.2 min, and finally equilibration for 2.8 min before injection of next sample. The column temperature was set at 50 °C. The software Xcalibur version 2.0 was used to control the instrument and collect data. The electrospray ionization source was fitted with a stainless steel capillary (100 μm i.d.). Nitrogen was used as both the sheath gas and the auxiliary gas. The ion transfer tube temperature was 300 °C. The spray voltage, tube lens voltage, and pressure of sheath gas and auxiliary gas were optimized to achieve maximal response using the test compounds mixing with the mobile phase A (50%) and B (50%) at a flow rate of 0.8 mL/min. Collision-induced dissociation was performed on VU0357017, VU0184670, and internal standard under 1.0 mTorr of argon. Selected reaction monitoring was carried out using the transitions from m/z 320 to 148 for VU0357017, m/z 334 to 162 for VU0184670, and m/z 310 to 223 for VU-178 (internal standard). The calibration curves were constructed and linear response was obtained in the range of 10−2000 ng/mL by spiking known amounts of analytes in blank brain homogenates and plasma.

The final PK parameters were calculated by noncompartmental analysis using WinNonlin software (version 5.1, Pharsight Inc.).

[^{3}H]-NMS Competition Binding

Membranes were prepared from M_1-, M_2-, M_3-, M_4-, and M_5-expressing CHO cells as previously described (*42*). Binding reactions contained 0.1 nM [^{3}H]-NMS and 20 μg of membrane and compound or 1 μM atropine (to define nonspecific binding) in a total volume of 500 μL. Compounds were serially diluted in DMSO-matched assay buffer (100 mM NaCl, 10 mM $MgCl_2$, 20 mM HEPES, pH 7.4) to give a final DMSO concentration of 0.3% in the binding reaction. Binding reactions were incubated for 2 h at room temperature on a Lab-line Titer plate shaker at setting 7 (~750 rpm). Reactions were stopped and membranes collected onto 96-well Barex microplates with GF/B filter (1 μm pore size) using a Brandel harvester and washed 3× with ice-cold harvesting buffer (50 mM Tris-HCl, 0.9% NaCl, pH 7.4). Filter plates were dried overnight and counted in a PerkinElmer TopCount scintillation counter (PerkinElmer Life and Analytical Sciences). Actual [^{3}H]-NMS concentrations were back-calculated after counting aliquots of 5× [^{3}H]-NMS added to the reaction. Radioligand depletion was routinely kept to approximately 10% or less.

VU0184670 M_1 Receptor Docking

Comparative models were generated for the M_1 receptor (manuscript in preparation) based on the X-ray crystal structure of the β2 adrenergic receptor (ref *43*; PDB ID 2RH1). A low-energy three-dimensional starting structure for the VU0184670 allosteric agonist was generated via gradient-based energy minimization using the Merck MMFF94 force field (MOE, Chemical Computing Group). The small molecule was initially placed manually into the third extracellular loop region of the M_1 receptor near the first helical turn of transmembrane span seven near residues E401 and E397 to reflect a putative interaction from loss-of-function mutagenesis data in an M_1 K392D/E397V/E401H triple mutant. ROSETTALIGAND (ref *44*) was then applied in a flexible ligand docking protocol to stochastically sample conformational space inside a 5 Å cube centered on this putative binding site for the allosteric agonist to identify low-energy, physically plausbile protein−ligand complexes. ROSETTALIGAND simultaneously placed probable side-chain amino acid rotamer conformations around the ligand and optimized the randomly sampled flexible ligand pose using a Metropolis Monte Carlo simulated annealing algorithm. The energy function used for scoring the models contained terms for van der Waals attractive and repulsive forces, statistical energy derived from the probability of observing a side-chain conformation in the PDB, hydrogen bonding, electrostatic interactions between amino acid pairs, and solvation to assess the effects of both protein−protein and protein−ligand side-chain interactions. Approximately 5000 docked complexes were generated, and the 1000 best scoring

DOI: 10.1021/cn900003h | *ACS Chem. Neurosci.* (2010), *1*, 104–121

models with the lowest energy ligand−protein interface scores were clustered based on ligand conformation and binding pose to identify potential M_1 receptor interactions with VU0184670. Cluster centers were visually inspected in PyMol (DeLano Scientific) to generate mechanistic hypotheses for allosteric agonist recognition and for the prediction of site-directed mutants to test putative M_1 receptor/VU0184670 interactions.

Site-Directed Mutagenesis of the M_1 Receptor

EE397/401DD, E397D, E401D, and E401A M_1 receptor mutants were all generated from a pcDNA3.1$^+$ vector containing WT rM_1 cDNA template using Stratagene's QuikChange XL site-directed mutagenesis kit (La Jolla, CA). For each PCR reaction, 10 ng of dsDNA template was amplified with 125 ng each of forward and reverse primer in a total reaction volume of 50 μL according to Stratagene's protocol. Reactions were cycled according to the following thermocycler program:

segment	cycles	temperature (°C)	time
1	1	95	1 min
2	18	95	50 s
		60	50 s
		68	4.5 min
3	1	68	7 min

Primers used to generate each mutation are listed 5′ to 3′ in the following table:

Primer	Sequence 5′ to 3′	Length (bp)
rM_1 E397D-Fwd	TGCAAGGACTG-CGTGCCCGACA-CCCTGTGGGAGCT	35
rM_1 E397D-Rev	AGCTCCCACAGG-GTGTCGGGCAC-GCAGTCCTTGCA	35
rM_1 E401D-Fwd	GAGACCCTGTGG-GACCTGGGCTACT	25
rM_1 E401D-Rev	AGTAGCCCAGGT-CCCACAGGGTCTC	25
rM_1 E401A-Fwd	GAGACCCTGTGGG-CGC TGGGCTACT	25
rM_1 E401A-Rev	AGTAGCCCAGCGC-CC ACAGGGTCTC	25

PCR reactions were checked for amplification products by agarose gel electrophoresis following reaction. Aliquots (45 μL) of PCR reaction were then utilized to transform 200 μL of DH5α *Escherichia coli* cells. These cells were then heat shocked for 1.5 min at 42 °C, after which they were immediately placed on ice, 800 μL LB (containing 10 g triptone; 5 g yeast extract; 5 g NaCl) was added, and the tubes were placed back on ice 2 min. Tubes were then incubated with shaking 45 min at 37 °C, and the transformation reactions were then pulse-spun down, resuspended in 50 μL of LB, and plated on LB-Ampicillin plates. The plates were then incubated overnight at 37 °C, after which three colonies for each mutant were picked for growth in LB-Amp liquid cultures for miniprep. Minipreps were conducted using QIAprep spin miniprep kit according to the manufacturer's protocol, and the resulting purified mutant cDNAs were verified by sequencing. Following introduction of the E397D single point mutation, the EE397/401DD double mutant was generated by repetition of the aforementioned procedure using E401D primers. One correct mutant for each mutation was then selected for growth in 250 mL of LB-Amp liquid cultures for a maxiprep using Qiagen's Maxiprep Kit according to the manufacturer's protocol. K392D/E97V/E401H, K392D, E397V, E401H mutants were generated as previously described (*26*).

Ten micrograms of each resulting mutant rM_1 cDNA was then used to transfect CHO-K1 cells (ATCC) using Fugene transfection reagent (Roche). Fugene 6 (36 μL) was added dropwise to 600 μL of Opti-MEM (Invitrogen) reduced serum medium and incubated at room temperature for 5 min. Following incubation, this mixture was added dropwise to 10 μg of mutant rM_1 cDNA in a separate tube and incubated for 15 min. The mixture was then added dropwise to a 50−80% confluent 100 mm dish of CHO-K1 cells, and the cells were grown to confluency overnight at 37 °C. Cells were then plated as described for Ca^{2+} assays.

Whole Cell Patch Clamping

Transverse hippocampal slices were prepared from Sprague−Dawley rats (postnatal day 18−24). Rats were anesthetized with isoflurane and decapitated. The brain was rapidly removed from the skull and submerged in ice-cold modified artificial cerebrospinal fluid (ACSF), which was bubbled with 95% O_2/5% CO_2, composed of (in mM) 230 sucrose, 2.5 KCl, 0.5 $CaCl_2$, 6 $MgSO_4$, 1.25 NaH_2PO_4, 26 $NaHCO_3$, and 10 D-glucose. The brain was blocked in the horizontal plane, glued to the stage of a vibratome (Vibratome, St. Louis, MO) that was filled with ice-cold modified ACSF, and cut at 290 μm. Slices were then incubated in oxygenated normal ACSF (in mM, 126 NaCl, 2.5 KCl, 3 $CaCl_2$, 1 $MgSO_4$, 1.25 NaH_2PO_4, 26 $NaHCO_3$, and 10 D-glucose) at 31−32 °C for 30 min and maintained at room temperature afterward until transferred individually to a fully submerged recording chamber that was continuously perfused with oxygenated ACSF at ∼30 °C.

Whole-cell recordings were made from visually identified hippocampal CA1 pyramidal neuron soma under an Olympus BX50WI upright microscope (Olympus, Lake Success, NY). A 40× water immersion objective coupled with Hoffman optics and video system was used to visualize individual CA1 pyramidal cells. A MultiClamp 700B amplifier (Molecular Devices, Union City, CA) was used for voltage-clamp recordings. Patch pipettes (4−6 MΩ) were prepared from borosilicate glass (World Precision Instrument, Sarasota, FL) using a Narashige vertical patch pipet puller (Narashige, Japan) and filled with the pipet solution containing (in mM) 130 $CsMeSO_2$, 1 NaCl, 1 $MgCl_2$, 0.035 $CaCl_2$, 10

DOI: 10.1021/cn900003h | *ACS Chem. Neurosci.* (2010), *1*, 104–121

HEPES, 0.05 EGTA, 4 Mg-ATP, and 0.3 Na-GTP. The pH of the pipet solution was adjusted to 7.3 with 1 M CsOH, and osmolality was adjusted to ~295 mOsm/kg. Cells were voltage-clamped at −60 mV and NMDA receptor-mediated currents were induced by pressure ejection of 1 mM NMDA to the soma of the recorded cell through a patch pipet using a Picospritzer II (General Valve, Fairfield, NJ). The experiment was carried out in the presence of tetrodotoxin (0.5−1 μM) to block voltage-gated sodium channels. All drugs were bath applied. Data acquisition and analysis were performed using a PC computer equipped with pCLAMP software (Molecular Devices, Union City, CA). Data are presented as percentage of the control value. Statistical analysis was performed using two-tailed paired Student's *t*-test, and *p*-values less than 0.05 ($p < 0.05$) were considered to be significant. Data are presented as mean ± SEM.

Data and Statistical Analysis

Data analysis was carried out utilitzing the GraphPad Prism 4.0 software package. Statistical analyses and nonlinear curve fits were carried out utilizing built in functions. Data are plotted as mean ± SEM unless otherwise specified.

Animals

Experiments were conducted in accordance with the US National Institutes of Health regulations of animal care and approved by the Institutional Animal Care and Use Committee, Vanderbilt University Medical Center. Subjects were housed in groups of two per cage in a large colony room under a 12-h light−dark cycle (lights on at 6:00 a.m.) with food and water provided *ad libitum*.

Contextual Fear Conditioning

Contextual fear conditioning studies were conducted in conditioning chambers housed in a sound-attenuating cubicle (Med Associates, St. Albans, VT) with a fluorescent light mounted on the back wall of the cubicle to provide illumination for the chamber. Stainless steel grid floors connected to shock scramblers and generators delivered the 0.5 mA unconditioned stimulus. A digital video camera mounted on the front wall of the cubicle was interfaced with a PC equipped with Video Freeze software (MED-VFC-RS, Med Associates), which incorporated a pixel-based method to measure and quantify freezing behavior. Based on previous studies, the motion threshold was set at 120 arbitrary units, 5-s freeze duration. All trials were recorded at 30 frames per second. In addition, 1 mL of a 10% vanilla extract solution was applied to the conditioning chamber grid floor to provide an olfactory cue.

Male Sprague−Dawley rats (Harlan Sprague−Dawley, Indianapolis, IN.), weighing 380−420 g, were handled and injected with vehicle for two days prior to training. On training day, rats were habituated for 30 min in the training room. Based on the PK studies with VU0357017, rats were pretreated for 30 min with either vehicle (i.p.) or a dose of VU0357017 (1−10 mg/kg, i.p.) prior to the training session. Rats were then pretreated for 15 min with either vehicle (sc) or scopolamine (0.2 mg/kg, sc). Rats were then placed in the conditioning chamber and given a 2.5 min habituation, followed by two shock-context pairing trials (1 s, 0.5 mA). A 2.5 min intertrial interval (ITI) separated each footshock. After the second shock pairing, the rat remained in the chamber for an additional 2 min without shock stimuli. All rats received the same conditioned freezing training protocol.

Approximately 24 h after training, the magnitude of contextual fear conditioning response was tested by placing the rats back into the same conditioning chambers with identical visual and odor cues and measuring freezing behavior in the absence of any shock stimuli for a 7 min period equivalent to the duration of the training session. Memory of the fear response 24 h after training was assessed by recording the amount of freezing response in the testing chamber environment. Freezing was defined as a motionless posture, except for respiratory movements and calculated as the percent of freezing behavior for the entire training session. Data were analyzed using a one-way analysis of variance, and if significant ($p < 0.05$), all dose groups were compared with the vehicle/scopolamine treated group using a Dunnett's test.

Supporting Information Available

Panlabs Ancillary Pharmacology Table, Impact of M_1 site-directed mutagenesis on VU0184670 agonist activity and pharmacokinetics of VU0184670 and VU0357017. This material is available free of charge via the Internet at http://pubs.acs.org.

Author Information

Corresponding Author

* Corresponding author. E-mail: craig.lindsley@vanderbilt.edu. Phone. 615-322-8700. Fax: 615-343-6532.

Author Contributions

Professors Lindsley, Weaver, Conn, and Meiler oversaw and designed the chemistry, HTS, molecular pharmacology, and modeling, respectively.
Mr. Lebois performed synthetic chemistry, in vitro molecular pharmacology, and mutagenesis work.
Mr. Bridges performed synthetic chemistry and in vitro molecular pharmacology.
Professor Niswender oversaw elements of the HTS and the in vitro molecular pharmacology.
Dr. Lewis conducted the HTS.
Dr. Dawson performed the molecular modeling.
Mr. Kennedy performed synthetic chemistry and scaled-up key compounds for *in vivo* studies.
Mr. Kane performed the cognition studies in rats.
Professor Jones oversaw and interpreted the data from the cognition studies in rats.
Professor Xiang performed the NMDA/electrophysiology studies.
Dr. Jadhav and Dr. Yin performed the in vivo PK and brain/plasma studies as well as the analytical chemistry for these samples.

Funding Sources

The authors thank the NIH and NIMH (Grant RO1 MH082867-01 and the MLPCN, Grant U54MH084659-01) for support of our programs. The authors further acknowledge

DOI: 10.1021/cn900003h | *ACS Chem. Neurosci.* (2010), *1*, 104–121

the support of a Vanderbilt Institute of Chemical Biology Pilot Project Grant and the Alzheimer's Association (Grant IIRG-07-57131) and T.M.B. acknowledges an ITTD (Grant T90-DA022873) predoctoral training grant.

Notes

C.W.L. receives funding from NIH, NIMH, NIDA, the Alzheimer's Association, the Michael J. Fox Foundation, Seaside Therapeutics, and Johnson&Johnson.
C.D.W. receives funding from NIH, NIMH, NIDA, the Michael J. Fox Foundation, Seaside Therapeutics, and Johnson&Johnson.
P.J.C. receives funding from NIH, NIMH, NIDA, the Michael J. Fox Foundation, Seaside Therapeutics, and Johnson&Johnson.

Abbreviations

VU0184670, ethyl 4-(2-benzamidoethylamino)piperidine-1-carboxylate; VU0357017, ethyl 4-(2-(2-methylbenzamido)ethylamino)piperidine-1-carboxylate; ACh, acetylcholine; AD, Alzheimer's disease; ANOVA, analysis of variance; CNS, central nervous system; DIEA, diisopropylethyl amine; DCM, dichloromethane; DMF, dimethylformamide; FBS, fetal bovine serum; GPCRs, G-protein-coupled receptors; HEPES, *N*-2-hydroxyethylpiperazine-*N*′-2-ethanesulfonic acid; HTS, high-throughput screening; ip, intraperitoneally; mAChR, muscarinic acetylcholine receptor; M_1, muscarinic acetylcholine receptor subtype 1; nAChR, nicotinic acetylcholine receptors; NMDA, *N*-methyl-D-aspartate; PAM, positive allosteric modulator; PCR, polymerase chain reaction; PS-DIEA, polymer-supported diisopropylethylamine; MP-BH$(OAc)_3$, macroporous triacetoxyborohydride; SAR, structure−activity-relationship; sc, subcutaneously; TFA, trifluoroacetic acid; WT, wild-type.

References

1. Levey, A. I. (1993) Immunological localization of M1-M5 muscarinic acetylcholine receptors in peripheral-tissues and brain. *Life Sci. 52*, 441–448.

2. Abrams, P., Andersson, K. E., Buccafusco, J. J., Chapple, C., Chet de Groat, W., Fryer, A. D., Kay, G., Laties, A., Nathanson, N. M., Pasricha, P. J., and Wein, A. (2006) Muscarinic receptors: Their distribution and function in body systems, and the implications for treating overactive bladder. *Br. J. Pharmacol. 148*, 565–578.

3. Volpicelli, L. A., and Levey, A. I. (2004) Muscarinic acetylcholine receptor subtypes in cerebral cortex and hippocampus. *Prog. Brain Res. 145*, 59–66.

4. Felder, C. C., Porter, A. C., Skillman, T. L., Zhang, L., Bymaster, F. P., Nathanson, N. M., Hamilton, S. E., Gomeza, J., Wess, J., and McKinzie, D. L. (2001) Elucidating the role of muscarinic receptors in psychosis. *Life Sci. 68* (22−23), 2605–2613.

5. Anagnostaras, S. G., Murphy, G. G., Hamilton, S. E., Mitchell, S. L., Rahnama, N. P., Nathanson, N. M., and Silva, A. (2003) Selective cognitive dysfunction in acetylcholine M1 muscarinic receptor mutant mice. *Nat. Neurosci. 6*, 51–58.

6. Wess, J., Eglen, R. M., and Gautam, D. (2007) Muscarinic acetylcholine receptors: Mutant mice provide new insights for drug development. *Nat. Rev. Drug Discov. 6*, 721–733.

7. Bartus, R. T. (2000) On neurodegenerative diseases, models, and treatment strategies: Lessons learned and lessons forgotten a generation following the cholinergic hypothesis. *Exp. Neurol. 163*, 495–529.

8. Langmead, C. J., Watson, J., and Reavill, C. (2008) Muscarinic acetylcholine receptors as CNS drug targets. *Pharmacol. Ther. 117*, 232–243.

9. Fisher, A. (2008) M1 muscarinic agonists target major hallmarks of Alzheimer's Disease -- the pivotal role of brain M1 receptors. *Neurodegener. Dis. 5*, 237–240.

10. Raedler, T. J., Bymaster, F. P., Tandon, R., Copolov, D., and Dean, B. (2007) Towards a muscarinic hypothesis of schizophrenia. *Mol. Psychiatry 12*, 232–246.

11. Shekhar, A., Potter, W. Z., Lightfoot, J., Lienemann, J., Dube, S., Mallinckrodt, C., Bymaster, F. P., McKinzie, D. L., and Felder, C. C. (2008) Selective muscarinic receptor agonist Xanomeline as a novel treatment approach for schizophrenia. *Am. J. Psychiatry 165*, 1033–1039.

12. Scarr, E., Sundrarn, S., Keriakous, D., and Dean, B. (2007) Altered hippocampal muscarinic M4, but not M1, receptor expression from subjects with schizophrenia. *Biol. Psychiatry 61*, 1161–1170.

13. Heinrich, J. N., Butera, J. A., Carrick, T., Kramer, A., Kowal, D., Lock, T., Marquis, K. L., Pausch, M. H., Popiolek, M., Sun, S. C., Tseng, E., Uveges, A. J., and Mayer, S. C. (2009) Pharmacological comparison of muscarinic ligands: Historical versus more recent muscarinic M1-preferring receptor agonists. *Eur. J. Pharmacol. 605*, 53–56.

14. Mirza, N. R., Peters, D., and Sparks, R. G. (2003) Xanomeline and the antipsychotic potential of muscarinic receptor subtype selective agonists. *CNS Drug Rev. 9* (2), 159–186.

15. Marino, M. J., Rouse, S. T., Levey, A. I., Potter, L. T., and Conn, P. J. (1998) Activation of the genetically defined m1 muscarinic receptor potentiates N-methyl-d-aspartate (NMDA) receptor currents in hippocampal pyramidal cells. *Proc. Natl. Acad. Sci. U.S.A. 95*, 11465–11470.

16. Sur, C., Mallorga, P. J., Wittmann, M., Jacobson, M. A., Pascarella, D., Williams, J. B., Brandish, P. E., Pettibone, D. J., Scolnick, E. M., and Conn, P. J. (2003) N-desmethylclozapine, an allosteric agonist at muscarinic 1 receptor, potentiates N-methyl-d-aspartate receptor activity. *Proc. Natl. Acad. Sci. U.S.A. 100*, 13674–13679.

17. Conn, P. J., Jones, C. K., and Lindsley, C. W. (2009) Subtype-selective allosteric modulators of muscarinic receptors for the treatment of CNS disorders. *Trends Pharmacol. Sci. 30*, 148–155.

18. Jeffrey Conn, P., Christopoulos, A., and Lindsley, C. W. (2009) Allosteric modulators of GPCRs: A novel approach

DOI: 10.1021/cn900003h | *ACS Chem. Neurosci.* (2010), *1*, 104–121

for the treatment of CNS disorders. *Nat. Rev. Drug Discovery 8*, 41–54.

19. Pakrasi, S., Colloby, S. J., Firbank, M. J., Perry, E. K., Wyper, D. J., Owens, J., McKeith, I. G., Williams, E. D., and O'Brien, J. T. (2007) Muscarinic acetylcholine receptor status in Alzheimer's disease assessed using (R, R) 123I-QNB SPECT. *J. Neurol. 254*, 907–913.

20. Shinoe, T., Matsui, M., Taketo, M. M., and Manabe, T. (2005) Modulation of synaptic plasticity by physiological activation of M1 muscarinic acetylcholine receptors in the mouse hippocampus. *J. Neurosci. 25*, 11194–11200.

21. Jones, C. K., Brady, A. E., Davis, A. A., Xiang, Z., Bubser, M., Tantawy, M. N., Kane, A. S., Bridges, T. M., Kennedy, J. P., Bradley, S. R., Peterson, T. E., Ansari, M. W., Baldwin, R. M., Kessler, R. M., Deutch, A. Y., Lah, J. J., Levey, A. I., Lindsley, C. W., and Conn, P. J. (2008) Novel selective allosteric activator of the M1 muscarinic acetylcholine receptor regulates amyloid processing and produces antipsychotic-like activity in rats. *J. Neurosci. 28*, 10422–10433.

22. Bodick, N. C., Offen, W. W., Levey, A. I., Cutler, N. R., Gauthier, S. G., Satlin, A., Shannon, H. E., Tollefson, G. D., Rasmussen, K., Bymaster, F. P., Hurley, D. J., Potter, W. Z., and Paul, S. M. (1997) Effects of xanomeline, a selective muscarinic receptor agonist, on cognitive function and behavioral symptoms in Alzheimer disease. *Arch. Neurol. 54*, 465–473.

23. Caccamo, A., Oddo, S., Billings, L. M., Green, K. N., Martinez-Coria, H., Fisher, A., and LaFerla, F. M. (2006) M1 receptors play a central role in modulating AD-like pathology in transgenic mice. *Neuron 49*, 671–682.

24. Lewis, J., Lebois, E. P., and Lindsley, C. W. (2008) Allosteric modulators of kinases and GPCRs. Design principles and structural diversity. *Curr. Opin. Chem. Biol. 12*, 269–280.

25. Bridges, T. M., and Lindsley, C. W. (2008) G-Protein-coupled receptors: From classical modes of modulation to allosteric mechanisms. *ACS Chem. Biol. 3*, 530–541.

26. Marlo, J. E., Niswender, C. M., Days, E. L., Bridges, T. M., Xiang, Y., Rodriguez, A. L., Shirey, J. K., Brady, A. E., Nalywajko, T., Luo, Q., Austin, C. A., Williams, M. B., Kim, K., Williams, R., Orton, D., Brown, H. A., Lindsley, C. W., Weaver, C. D., and Conn, P. J. (2009) Discovery and characterization of novel allosteric potentiators of M_1 muscarinic receptors reveals multiple modes of activity. *Mol. Pharmacol. 75* (3), 577–588.

27. Brady, A. E., Jones, C. K., Bridges, T. M., Kennedy, J. P., Thompson, A. D., Heiman, J. U., Breininger, M. L., Gentry, P. R., Yin, H., Jadhav, S. B., Shirey, J. K., and Conn, P. J. (2008) Centrally active allosteric potentiators of the M_4 muscarinic acetylcholine receptor reverse amphetamine-induced hyperlocomotor activity in rats. *J. Pharmacol. Exp. Ther. 327* (3), 941–953.

28. Bridges, T. M., Marlo, J. E., Niswender, C. M., Jones, C. K., Jadhav, S. B., Gentry, P. R., Plumley, H. K., Weaver, C. D., and Conn, P. J. (2009) Discovery of the first highly M5-preferring muscarinic acetylcholine receptor ligand, an M5 positive allosteric modulator derived from a series of 5-trifluoromethoxy *N*-benzyl isatins. *J. Med. Chem. 52*, 3445–3448.

29. Langmead, C. J., Fry, V. A. H., Forbes, I. T., Branch, C. L., Christopoulos, A. C., Wood, M. D., and Herdon, H. J. (2006) Probing the molecular mechanism of interaction between 4-n-butyl-1-[4-(2-methylphenyl)-4-oxo-1-butyl]-piperidine (AC-42) and the muscarinic M1 receptor: Direct pharmacological evidence that AC-42 is an allosteric agonist. *Mol. Pharmacol. 69*, 236–246.

30. Langmead, C. J., Austin, N. E., Branch, C. L., Brown, J. T., Buchanan, K. A., Davies, C. H., Forbes, I. T., Fry, V. A. H., Hagan, J. J., Herdon, J. J., Jones, G. A., Jeggo, R., Kew, J. N. C., Mazzali, A., Melarange, R., Patel, N., Pardoe, J., Randall, A. D., Roberts, C., Roopun, A., Starr, K. R., Teriakidis, A., Wood, M. D., Whittington, M., Wu, Z., and Watson, J. (2008) Characterization of a CNS penetrant, selective M1 muscarinic receptor agonist, 77-LH-28-1. *Br. J. Pharmacol. 154*, 1104–1115.

31. Spalding, T. A., Trotter, C., Skjaerbaek, N., Messier, T. L., Currier, E. A., Burstein, E. S., Li, D., Hacksell, U., and Brann, M. R. (2002) Discovery of an ectopic activation site on the M1 muscarinic receptor. *Mol. Pharmacol. 61*, 1297–1302.

32. Lebon, G., Langmead, C. J., Tehan, B. G., and Hulme, E. C. (2009) Mutagenic mapping suggests a novel binding mode for selective agonists of M1 muscarinic acetylcholine receptors. *Mol. Pharmacol. 75*, 331–341.

33. Chan, W. Y., McKinzie, D. L., Bose, S., Mitchell, S. N., Witkin, J. M., Thompson, R. C., Christopoulos, A. C., Lazareno, S., Birdsall, N. J. M., Bymaster, F. P., and Felder, C. C. (2008) Allosteric modulation of the muscarinic M4 receptor as an approach to treating schizophrenia. *Proc. Natl. Acad. Sci. U.S.A. 105*, 10978–10983.

34. Malenka, R. C., and Bear, M. F. (2004) LTP and LTD: An embarrassment of riches. *Neuron 44*, 5–21.

35. Origlia, N., Kuczewski, N., Aztiria, E., Gautam, D., Wess, J., and Domenici, L. (2006) Muscarinic acetylcholine receptor knockout mice show distinct synaptic plasticity impairments in the visual cortex. *J. Physiol.-London 577*, 829–840.

36. McCoy, P., Norton, T. T., and McMahon, L. L. (2008) Layer 2/3 synapses in monocular and binocular regions of tree shrew visual cortex express mAChR-dependent long-term depression and long-term potentiation. *J. Neurophysiol. 100*, 336–345.

37. Ibach, B., and Haen, E. (2004) Acetylcholinesterase inhibition in Alzheimer's Disease. *Curr. Pharm. Des. 10*, 231–251.

38. Lleo, A., Greenberg, S. M., and Growdon, J. H. (2006) Current pharmacotherapy for Alzheimer's Disease. *Annu. Rev. Med. 57*, 513–533.

39. Sheffler, D. J., Williams, R. W., Bridges, T. M., Xiang, Z., Kane, A. S., Byun, N. E., Jadhav, S., Mock, M. M., Zheng, F., Lewis, L. M., Jones, C. K., Niswender, C. M., Weaver, C. D., Lindsley, C. W., Conn, P. J. (2009) A novel selective muscarinic acetylcholine receptor subtype 1 (M_1 mAChR) antagonist reduces seizures without impairing hippocampal-dependent learning. *Mol. Pharmacol.* Epub April 30, 2009. DOI: 10.1124/mol.109.056531.

40. MLPCN Web site: https://mli.nih.gov/mli/mlpcn/.

41. Kennedy, J. P., Williams, L., Bridges, T. M., Daniels, R. N., Weaver, D., and Lindsley, C. W. (2008) Application of combinatorial chemistry science on modern drug discovery. *J. Comb. Chem. 10* (3), 345–354.

42. Shirey, J. K., Xiang, Z., Orton, D., Brady, A. E., Johnson, K. A., Williams, R., Ayala, J. E., Rodriguez, A. L., Wess, J., Weaver, D., Niswender, C. M., and Conn, P. J. (2008) An allosteric potentiator of M_4 mAChR modulates hippocampal synaptic transmission. *Nat. Chem. Biol. 4*, 42–50.

43. Cherezov, V., Rosenbaum, D. M., Hanson, M. A., Rasmussen, S. G. F., Thian, F. S., Kobilka, T. S., Choi, H., Kuhn, P., Weis, W. I., Kobilka, B. K., and Stevens, R. C. (2007) High-resolution crystal structure of an engineered human β2-adrenergic G protein-coupled receptor. *Science 318*, 1258–1265.

44. Meiler, J., and Baker, D. ROSETTALIGAND: protein-small molecule docking with full side-chain flexability. *Proteins 65* (3), 538–548.

Note Added after ASAP Publication

This paper was published on the Web on September 25, 2009, with an error in Figure 11. The figure has been replaced with the corrected version, and the paper was reposted on September 29, 2009.

DOI: 10.1021/cn900003h | *ACS Chem. Neurosci.* (2010), *1*, 104–121